Supporting Information

Mechanisms for High Selectivity in Hydrodeoxygenation of 5-Hydroxymethylfurfural over PtCo Nanocrystals

Jing Luo[a,†], Hongseok Yun[b,†], Alexander V. Mironenko[c,†], Konstantinos Goulas[c], Jennifer D. Lee[b], Matteo Monai[d], Cong Wang[a], Vassili Vorotnikov[c], Christopher B. Murray[b], Dionisios G. Vlachos[c], Paolo Fornasiero[d] and Raymond J. Gorte[a,*]

[a]Department of Chemical & Biomolecular Engineering, University of Pennsylvania
Philadelphia, PA 19104, United States
[b]Department of Chemistry, University of Pennsylvania
Philadelphia, PA 19104, United States
[c]Department of Chemical & Biomolecular Engineering, University of Delaware
Newark, DE 19716, United States
[d]Department of Chemical and Pharmaceutical Sciences, University of Trieste
Trieste, 34127, Italy

† These authors contribute equally.

* Corresponding Author: Raymond J. Gorte

  Email: gorte@seas.upenn.edu

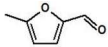**Table S1.** Yields of partially hydrogenated compounds for HDO of HMF at 120 ºC and 33 bar.
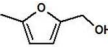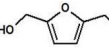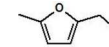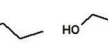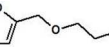
Catalyst	W/F (g·min/mL)						
Pt	0.0625	1.3	0	3.7	3.8	25.4	3.4
	0.25	0	0	2.1	2.7	17.0	2.7
	1	0	0	0	0	6.8	0
Pt₃Co	0.0625	0.8	0	4.8	3.2	23.5	2.6
	0.25	0	1.6	2.1	2.3	11.9	2.9
	1	0	0.8	0	0	5.2	0
Pt₃Co₂	0.0625	3.0	0	2.6	4.0	10.1	3.1
	0.25	2.3	2.4	11.5	3.7	14.2	4.0
	1	1.7	6.3	11.4	3.6	9.2	0

Table S2. Particle size distribution of Pt and Pt_3Co_2 nanocrystals.

	Pt nanocrystal size (nm)	Pt_3Co_2 nanocrystal size (nm)
As-synthesized	2.4 ± 0.2	3.7 ± 0.3
After surface treatment	2.5 ± 0.3	3.7 ± 0.3
After reaction	3.5 ± 0.7	3.8 ± 0.4

Table S3. Fitting of the EXAFS Pt and Co spectra. All distances in Angstroms.

Co EXAFS	Pt_3Co_2-400	Pt edge EXAFS	Pt_3Co_2-400	Pt_3Co_2-250
Co-Pt distance	2.645	Pt-Co distance	2.645 ± 0.005	2.646 ± 0.006
Co-Co distance	2.554 ± 0.013	Pt-Pt distance	2.730 ± 0.003	2.743 ± 0.002
Co-O distance	-	-	-	-
Co-Co CN	7.69 ± 1.93	Pt-Pt CN	8.02 ± 0.62	8.98 ± 0.57
Co-Pt CN	6.27 ± 0.98	Pt-Co CN	3.84 ± 0.47	2.88 ± 0.44
Co-O CN	-	-	-	-
R^2	0.007	R^2	0.002	0.001
ΔE_0 (eV)	-7.60 ± 0.93	ΔE_0 (eV)	6.47 ± 0.33	6.32 ± 0.30
σ^2 Pt-Co (x10^4)	90	σ^2 Pt-Co (x10^4)	90 ± 10	85 ± 12
σ^2 Co-Co (x10^4)	171 ± 31	σ^2 Pt-Pt (x10^4)	65 ± 4	54 ± 3

Table S4. Metal dispersions of alumina supported catalysts after 250°C and 400°C reduction, assuming CO/Pt=1 and no CO adsorption on Co atoms.

Sample	Dispersion (250°C reduction)	Dispersion (400°C reduction)
1-wt% Pt/Al$_2$O$_3$	19.4 %	12.6%
1-wt% Pt$_3$Co$_2$/Al$_2$O$_3$	0 %	8.8 %

Table S5. DFT reaction energies and barriers on a Co_3O_2/Pt(111) honeycomb surface. Index numbers correspond to structures in Figure S5. Forces were converged at 0.2 eV/Å level due to slow convergence.

Reaction	#	DFT reaction energy, eV	DFT reaction barrier, eV
Hydrogen activation			
$H_2 + * = H_2*$	-	-0.14	N/A
$H_2* = H_{Pt-Co}* - H_{Pt-Co}*$	1	-0.15	0.68
$H_2* = H_{Pt-Co}* - OH_{vac}*$	2	-0.41	1.19
$H_2* = 2OH_{vac}*$	3	-0.86	1.5
Vacancy formation			
$H_{Pt-Co}* - H_{Pt-Co}* = H_{Pt-Co}* - OH_{vac}*$	4	-0.29	1.26
$H_{Pt-Co}* - OH_{vac}* = H_2O_{vac}*$	5	+0.13	1.15
$H_2O_{vac}* = H_2O + *_{vac}$	-	+0.56	N/A
HMF-to-HMMF conversion			
$HMF + 2H_{Pt-Co}* = HMF-2H_{Pt-Co}*$	-	-0.80	N/A
$HMF-2H_{Pt-Co}* = BHMF*$	6	-0.56	0.84
$BHMF* = BHMF + *$	-	+0.91	N/A
$BHMF* = BHMFmOH*-OH*$	7	+0.93	1.19
$BHMFmOH*-OH* = HMMF*-O*$	8	-0.19	0.17
$HMMF*-O* = HMMF + O*$	-	+0.78	N/A
O removal			
$H_2 + O* = H_2*-O*$	-	-0.12	N/A
$H_2*-O* = H_{Pt}*-OH*$	9	-1.21	0.28[1]
$H_{Pt}*-OH* = H_2O*$	10	-0.90	0.23
$H_2O* = H_2O + *$	-	+0.41	N/A
BHMF-to-HMMF conversion on a vacancy			
$BHMF + *_{vac} = BHMF*_{vac}$	-	-1.32	N/A
$BHMF_{vac}* = BHMFmOH*-OH_{vac}*$	11	+0.10	N/A
$BHMFmOH*-OH_{vac}* = HMMF*$	12	-0.63	N/A
$HMMF* = HMMF + *$	-	+0.63	N/A

Notation:

* – intact honeycomb oxide surface;

$H_{Pt-Co}*$ – hydrogen atom bound to Pt and Co atoms in a bridging configuration;

$OH_{vac}*$ and $H_2O_{vac}*$ – OH and H_2O adsorbed on a vacancy;

$O*$, $OH*$, and H_2O* - O, OH, and H_2O adsorbed on an intact honeycomb surface between two Co atoms in a bridging configuration;

$*_{vac}$ – honeycomb oxide with a vacancy;

H_2*-O* – O* species with a H_2 molecule physisorbed nearby over a Pt atom

HMF – 5-(hydroxymethyl)furfural;

$HMF-2H_{Pt-Co}*$ – HMF co-adsorbed with two $H_{Pt-Co}*$ atoms;

BHMF – 2,5-bis(hydroxymethyl)furan;

BHMFmOH* - radical formed after removal of the hydroxyl side group from BHMF;

HMMF – 2-(hydroxymethyl)-5-methylfuran;

N/A – reaction barrier was not calculated

Table S6. Comparison of properties and numbers of surface atoms in Pt_3Co_2 and Pt_3Co NCs with a core/shell structure.

	Pt_3Co_2 (core/shell)	Pt_3Co (core/shell)
Nanoparticle size	3.7 nm	3.2 nm
Lattice constant	3.87 Å[1]	3.87 Å[1]
Bulk Co fraction	14.4 %	14.4 %[2]
Total number of atoms	1827	1168
Number of surface atoms	662[3]	491[3]
Number of surface Co atoms	547[4]	405[4]
Number of surface Co atoms available at given bulk Co fraction	547	184

[1]Calculated from XRD; [2]Assumed to be the same as for Pt_3Co_2; [3]Calculated for a close-packed surface; [4]Based on 70% of Co_3O_2-covered terrace sites and 30% of CoO-covered steps

Table S7. Comparison of estimated properties of three Pt_3Co_2 NCs: an alloy core/surface Co_3O_2 monolayer shell geometry, a Pt_3Co_2 random alloy, and a Pt NC of the same size.

		Pt_3Co_2 (core/shell)	Pt_3Co_2 (random alloy)	Pt
Nanoparticle size		3.7 nm	3.7 nm	3.7 nm
Lattice constant		3.87 Å[1]	3.77 Å[2]	3.92 Å
Bulk Co fraction		14.4 %	40 %	-
Total number of atoms		1827	1983	1754
Number of surface atoms		662 (546[3])	700	645
Number of subsurface atoms		524	-[4]	-[4]
Dispersion		36.3 %	35.3 %	36.8 %
Distribution of Co atoms in each part	Surface	74.8 %[3]	35.3 %	-
	Subsurface	10.3 %[3]	-[4]	-
	Bulk	14.9 %[3]	64.7 %	-
Distribution of Pt atoms in each part	Surface	0 %[3]	35.3 %	36.8 %
	Subsurface (under terraces)	22.8 %[3]	-[4]	-[4]
	Subsurface (under steps)	18.1 %[3]		
	Bulk	59.1 %[3]	64.7 %	63.2 %
Coordination numbers	Pt-Co	2.92	4.38[5]	-[5]
	Pt-Pt	8.91	6.57[5]	10.90[5]
	Pt-M	11.83	10.94[5]	10.90[5]

[1]Calculated based on XRD; [2]estimated based on the bulk composition and Vegard's law; [3]Assuming 70% of surface sites are present as a Co_3O_2 honeycomb structure; [4]subsurface atoms are considered part of the bulk, due to identical coordination; [5]for the Pt_3Co_2 random alloy and the Pt NC, $CN_{total} = 9$ in the surface and $CN_{total} = 12$ in the bulk.

Table S8. Calculation of the vacancy formation rate at conditions of kinetic measurements (160°C, 33 bar H_2) and catalyst pretreatment/XAS conditions (250°C, 1 bar H_2).

	250 °C, 1 bar H_2	160 °C, 33 bar H_2
$\Delta G_{H_2,ads}$, J/mol	$3.31 \cdot 10^4$	$2.16 \cdot 10^4$ *
$\Delta G^{\neq}_{O+H \to OH}$, J/mol	$1.17 \cdot 10^5$	$1.17 \cdot 10^5$
θ_{2H}	$4.95 \cdot 10^{-4}$	$8.19 \cdot 10^{-2}$
$k_{O+H \to OH}$, s^{-1}	$2.32 \cdot 10^1$	$6.42 \cdot 10^{-2}$
r, s^{-1}	$\mathbf{1.15 \cdot 10^{-2}}$	$\mathbf{5.26 \cdot 10^{-3}}$

*Gibbs free energy of reaction is given at 1 atm.
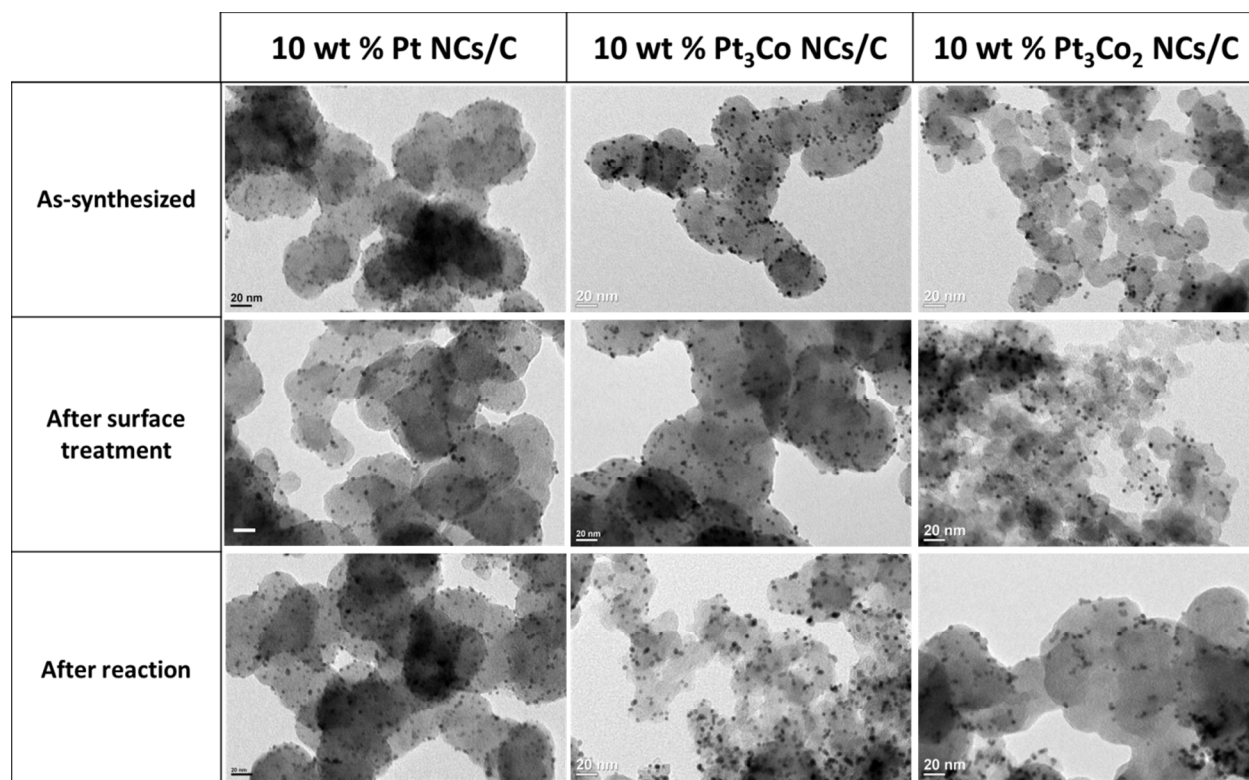
Figure S1. TEM images of as-synthesized NC catalyst on carbon support, after surface treatment, and after reaction.
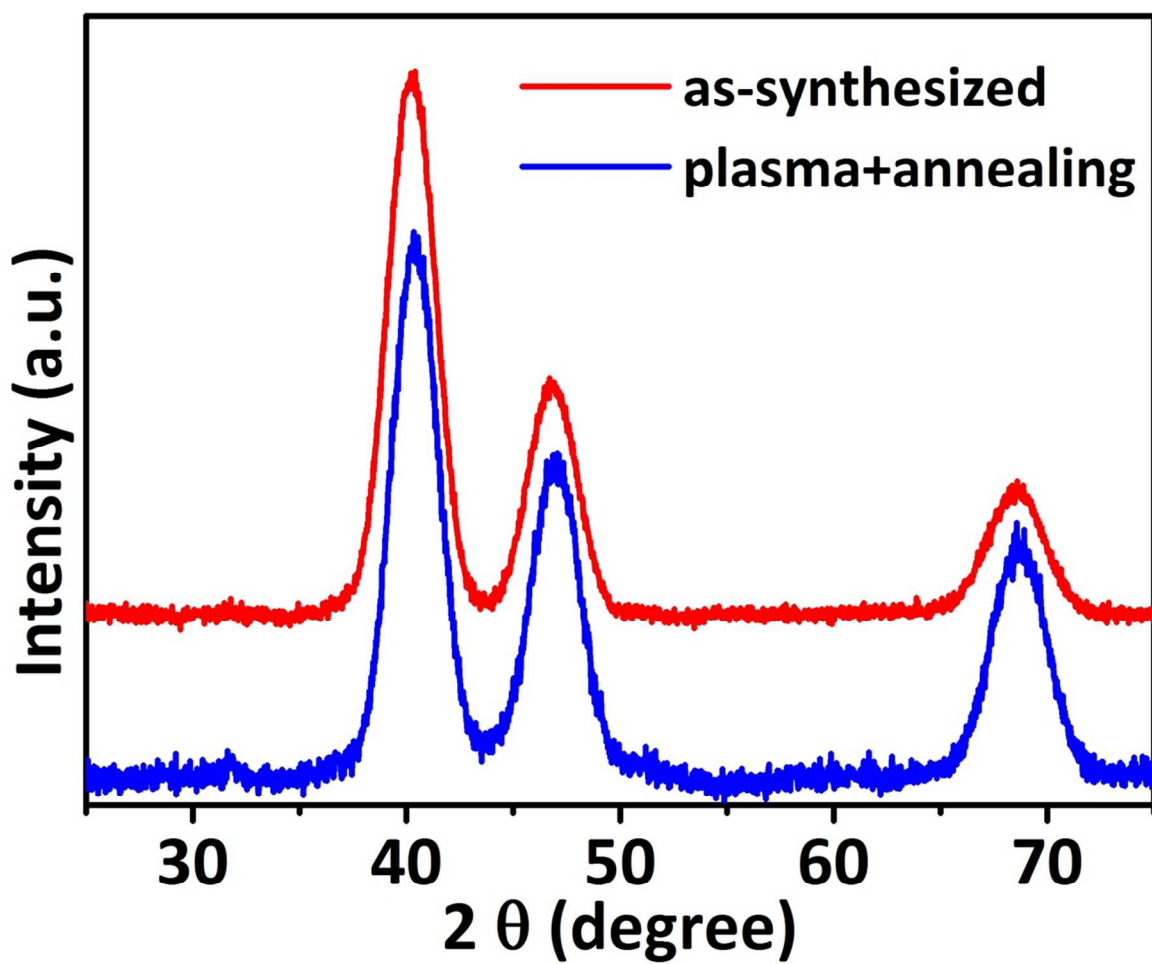
Figure S2. Wide angle x-ray scattering data of as-synthesized (red) and after surface cleaned (blue) Pt_3Co_2 NCs.
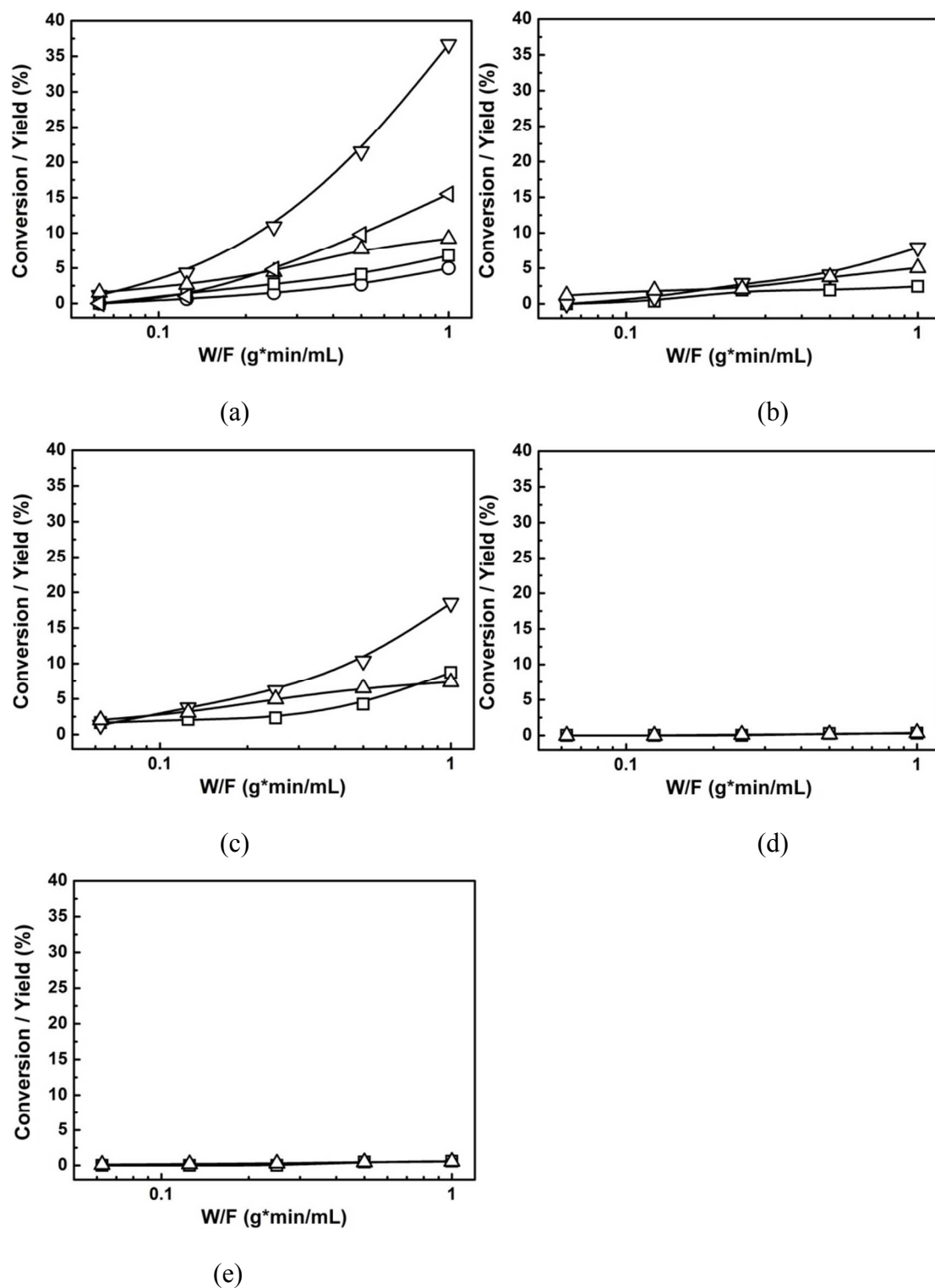
Figure S3. Yields of over-hydrogenated compounds as a function of space time at 33 bar: (a) 10-wt% Pt/C at 120 ºC (b) 10-wt% Pt₃Co/C at 120 ºC, (c) 10-wt% Pt₃Co/C at 160 ºC; (d) 10-wt% Pt₃Co₂/C at 120 ºC, (e) 10-wt% Pt₃Co₂/C at 160 ºC. ($\square$) DMTHF, ($\triangledown$) 2-hexanone, 2-hexanol and 2-propoxyhexane, ($\triangle$) 2,5-hexandione, 2,5-dipropoxyhexane, ($\bigcirc$) hexane, ($\triangleleft$) unidentified
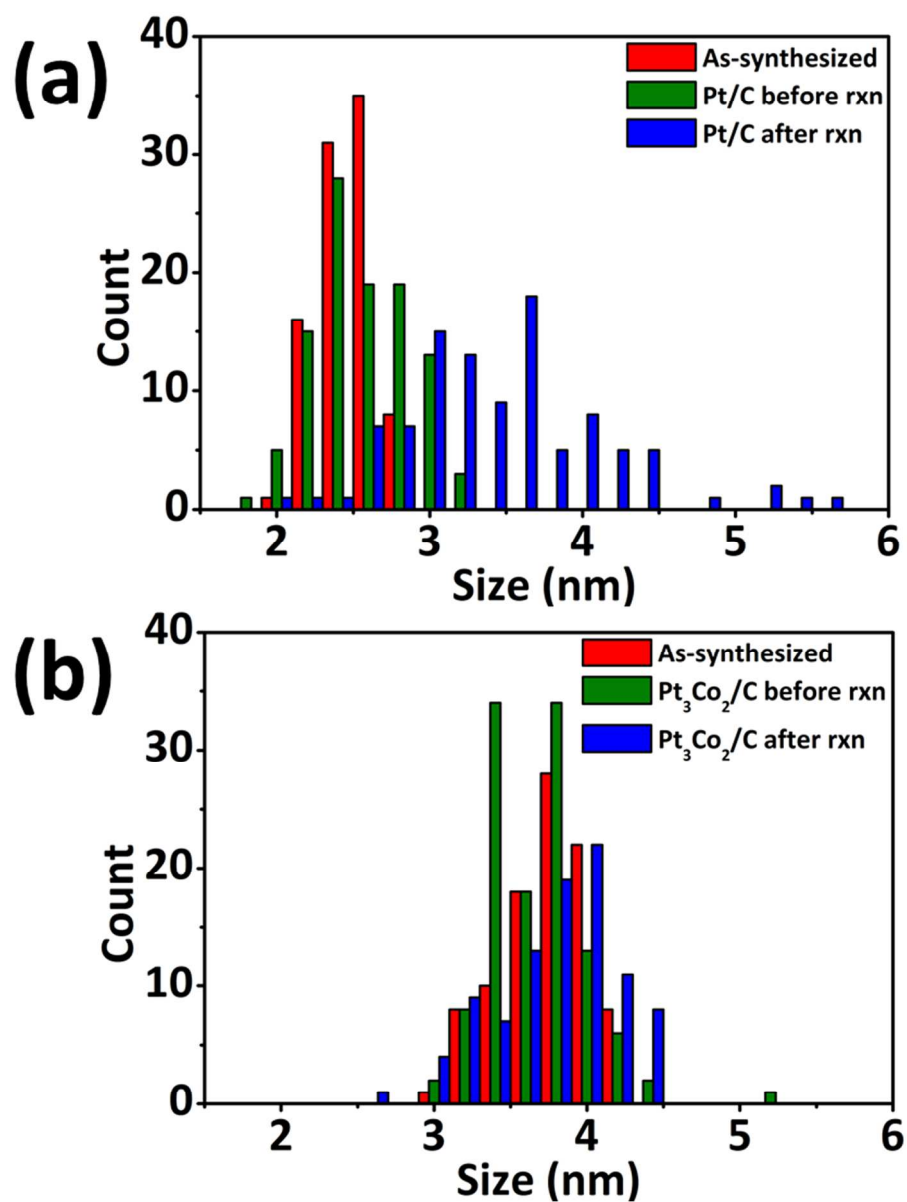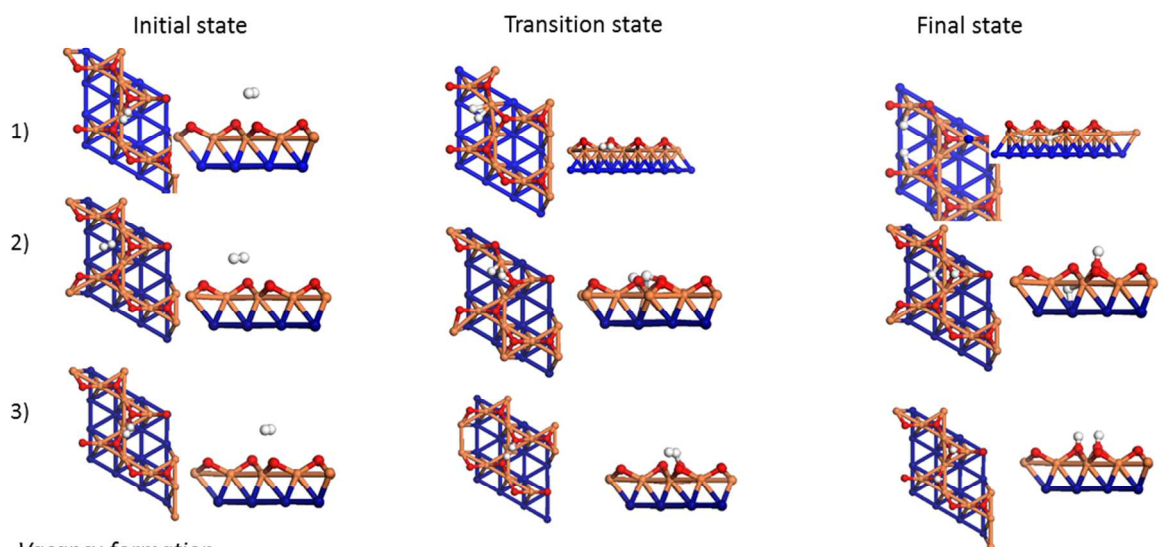
Figure S4. The particle size distribution of (a) Pt and (b) Pt_3Co_2 nanocrystals before and after the hydrodeoxygenation reactions.
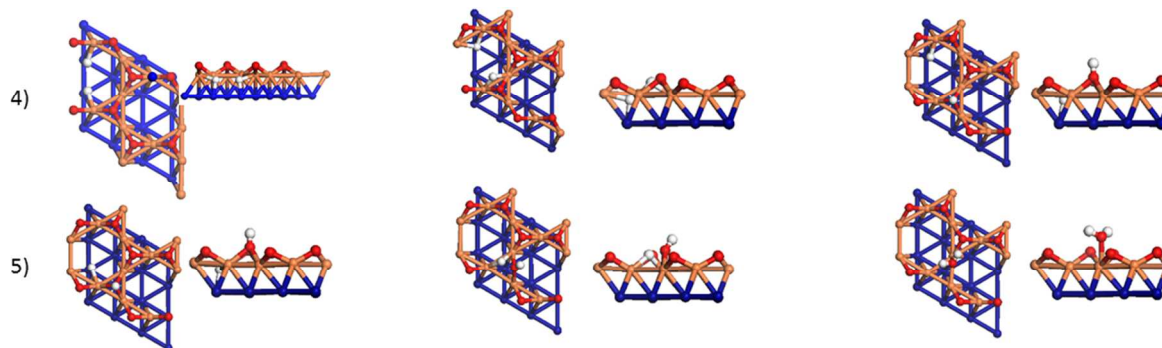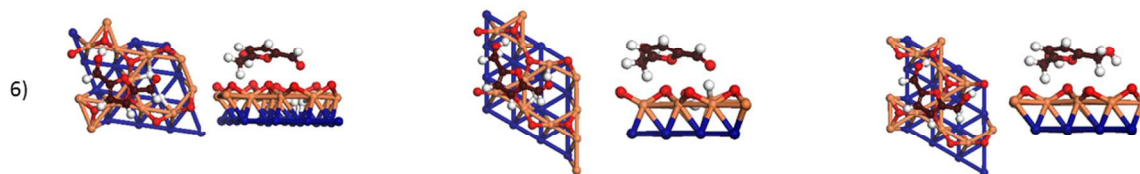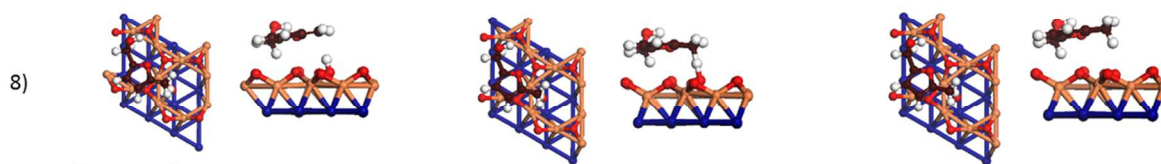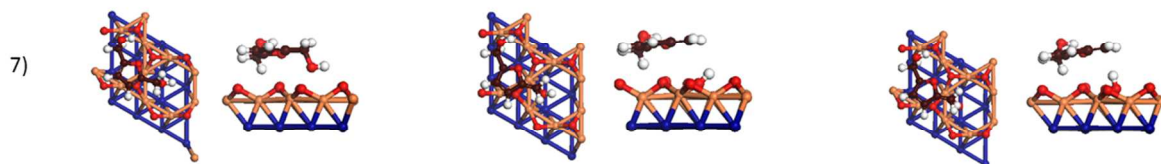
Figure S5. Optimized structures of initial, transition, and final states that correspond to reactions in Table S5. Blue atoms - Pt, orange atoms - Co, red atoms - oxygen, brown atoms - carbon. The figure continues on the next page.

HMF-to-BHMF conversion

6)

BHMF-to-BHMMF conversion

7)

8)

O removal

9)

10)

BHMF-to-BHMMF conversion over a vacancy
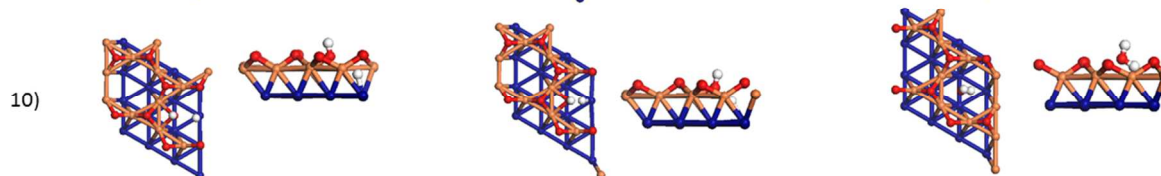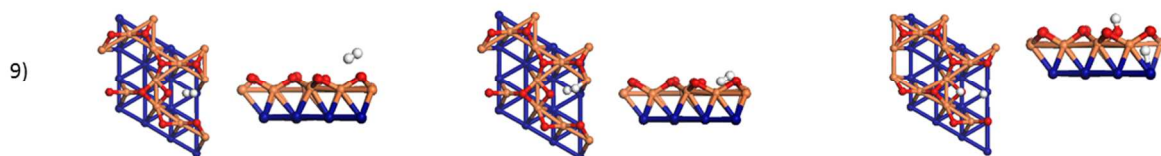
11)   N/A
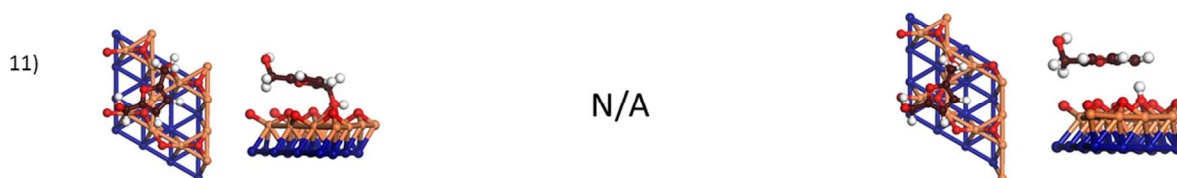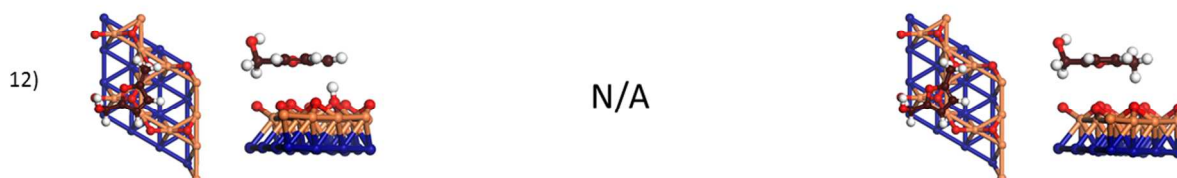
12)   N/A

Figure S5. Follow the last page.
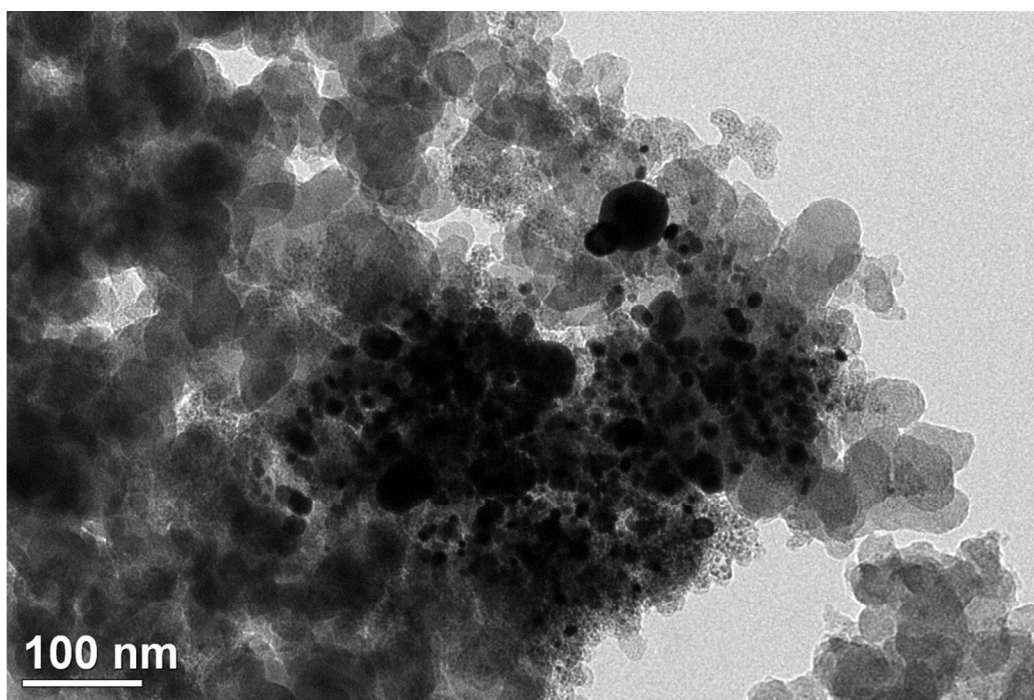
Figure S6. TEM images of 10-wt% Pt_3Co_2/C prepared by wet impregnation method.
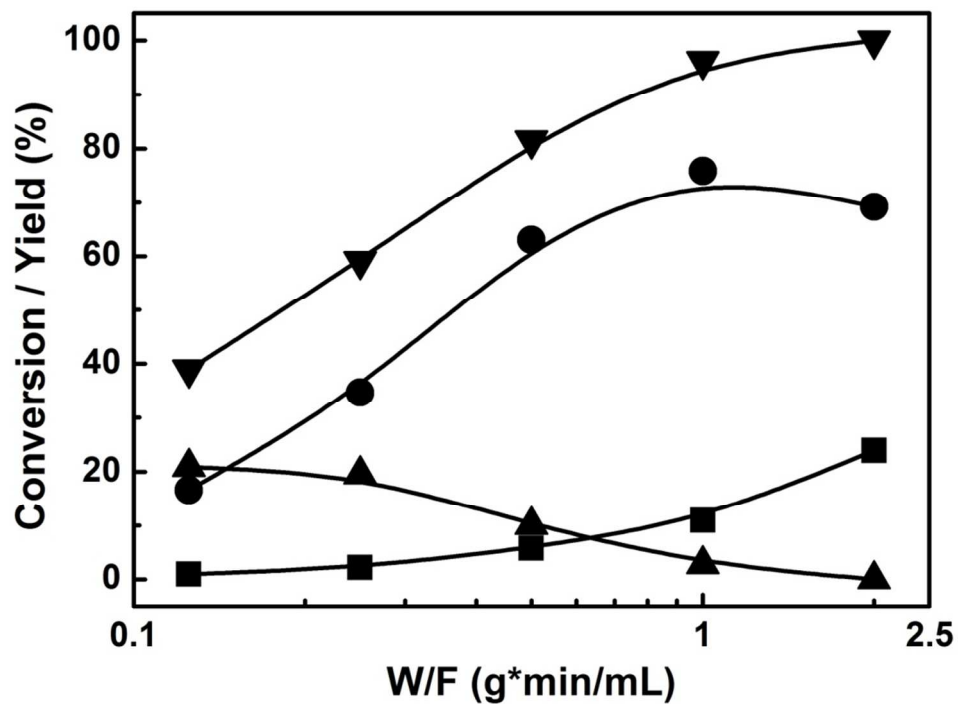
Figure S7. Conversion and product distribution for the HDO reaction of HMF over impregnated 10-wt% Pt_3Co_2/C, as a function of reactor space time. Reaction conditions: 33 bar and 160 ºC. (▼) HMF conversion, (▲) product group B, (●) DMF, (■) product group D
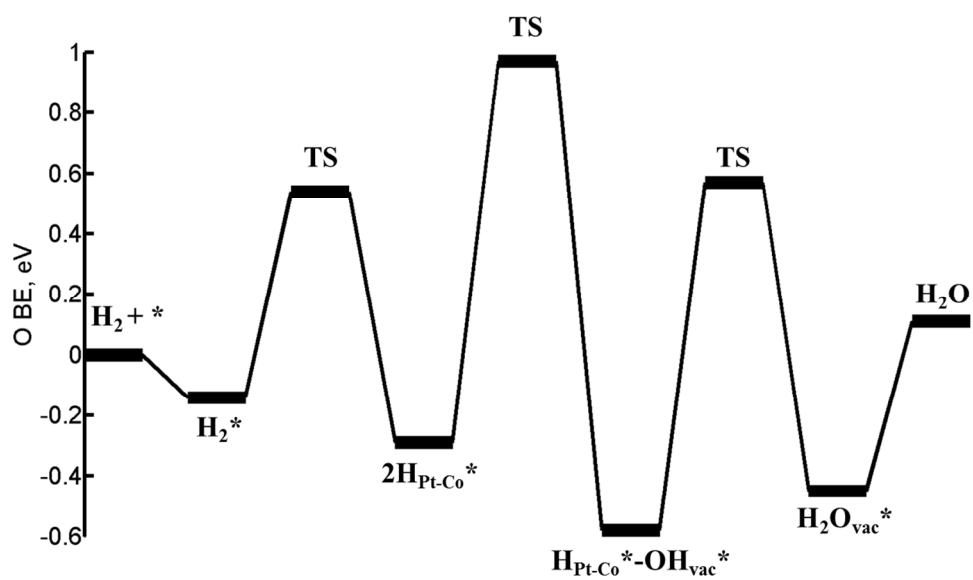
Figure S8. Energy diagram for vacancy formation. Notations correspond to Table S5.
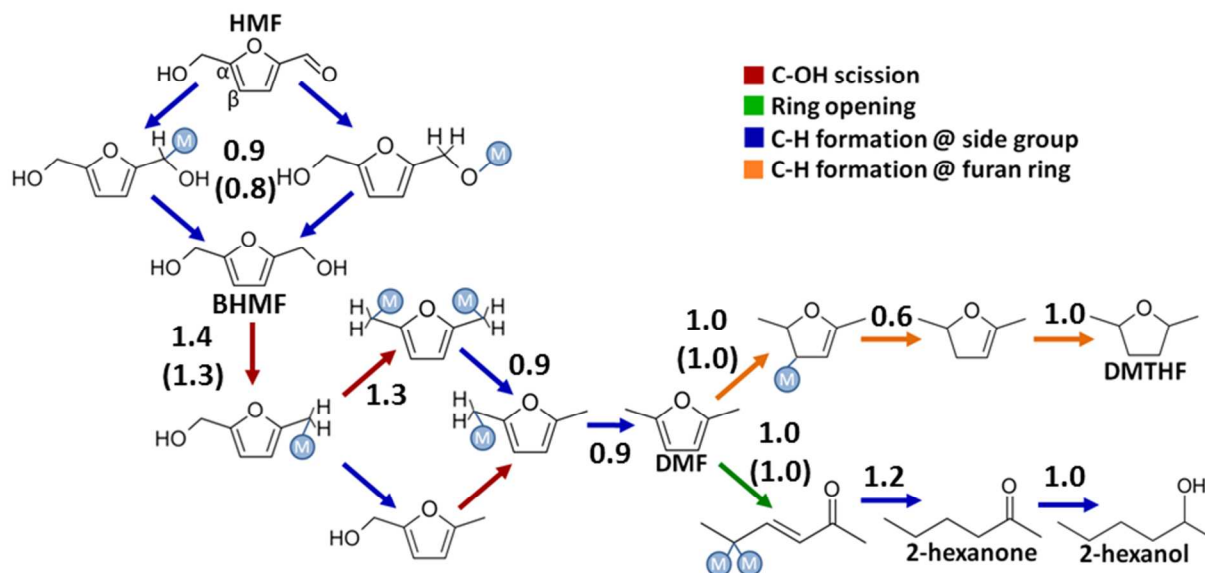
Figure S9. Overall reaction network considered for HMF hydrogenolysis to DMF and its side reactions. Numbers are the highest reaction barriers estimated using first principles screening methods[1]. Numbers in parentheses are DFT-refined values.

Section S1. Preparation of nanocrystal catalysts

To prepare 2.5 nm Pt NCs, 314 mg of platinum acetylacetonate (Acros, 98%) was dissolved in 40 mL of trioctylamine (Sigma-Aldrich, 97 %), 10.9 mL of oleylamine (Sigma-Aldrich, 70 %), 2.6 mL of oleic acid (Sigma-Aldrich, 90 %), and 0.9 mL of trioctylphosphine (Acros Organics, 97 %). The reaction mixture was kept under vacuum at 80 °C for 30 minutes and then heated up to 300 °C at a rate of 10 °C/min. After 30 minutes, the reaction mixture cooled down to room temperature. After then, into the reaction mixture, 40 mL of toluene was added. The mixture was divided into 6 centrifuge tubes (50 mL) and 30 mL of isopropanol and 5 mL of ethanol were added. After 2 minutes of centrifugation at 6000 rpm, the supernatant was removed and the precipitate was able to be re-dispersed in hexane or toluene. After washing the excess amount of oleic acid, oleylamine, and trioctylamine by isopropanol, the NCs were dispersed in toluene.

To synthesize 3.2 nm Pt_3Co NCs, we scaled up a method reported by Shevchenko *et al.*[4] 264 mg of platinum acetylacetonate was dissolved in 32 g of hexadecylamine (Acros Organics, 90 %) and 16 mL of diphenyl ether (Sigma-Aldrich, 99 %) in the presence of 672 mg of 1-adamantane carboxylic acid (Acros, 99 %) and 1.04 g of 1,2-hexadecanediol (HDD, Sigma-Aldrich). The reaction mixture was put under vacuum at 80 °C for 30 minutes and then heated at a rate of 10 °C/min. When the temperature reached to 170 °C, 334 mg of $Co_2(CO)_8$ (Acros, 95 %) dissolved in 3.2 mL of 1,2-dichlorobenzene was injected. The reaction mixture was heated further to 230 °C and kept for 40 minutes. After then, the reaction mixture was allowed to cool down and 50 mL of toluene was injected at 200 °C. When the temperature was cooled down to 90 °C, the reaction mixture was divided into 6 centrifuge tubes (50 mL) and 30 mL of isopropanol, which was prepared to be warm (~ 50 C°), was added to each centrifuge tube. After 2 minutes of centrifugation at 6000 rpm, the supernatant was removed and the precipitate was easily dispersible in non-polar solvent such as hexane and toluene. After washing the colloid with isopropanol 2-3 times, the NCs were kept in hexane.

For 3.6 nm Pt_3Co_2 NCs, we modified the reaction method for Pt_3Co NCs. 32 g of hexadecylamine was replaced by 41 mL of oleylamine, 16 mL of diphenyl ether by 16 mL of 1-octadecene (Acros, 90 %), and HDD was not added. After vacuum at 80 °C for 30 minutes, the reaction mixture was heated to 300 °C. At 170 °C, the same amount of $Co_2(CO)_8$ was injected. After 30 minutes at 300 °C, the reaction mixture cooled down to room temperature and 50 mL of hexane was added. The other washing process was same as described in the reaction for Pt_3Co NCs.

To prepare NC catalyst, NCs in 20 mL of hexane were mixed with carbon powder (Cabot, Vulcan XC72R) in a 50 mL centrifuge tube by sonication. The metal loading was 10 wt %. After 15 minutes of sonication, the solution was centrifuged at 6000 rpm for 1 minute. The supernatant should be transparent and removed. Then, the powder was washed with 20 mL of isopropanol and centrifuged again. Then, the powder was dried in a vacuum oven for overnight at 50 °C. To increase catalytic activity of NCs, the powder went through surface cleaning processes. For this purpose, the dry powder was treated with O_2 plasma for 15 minutes. After then, the powder was put into a furnace at 500 °C and taken out after 1 minute. The resulting powder was gone through all the HDO reactions.

Section S2. Estimation of average coordination numbers and oxidation state

We estimate average Pt coordination numbers of a core/shell nanoparticle for comparison with XAS results according to the following equation:

$$CN_{av} = x_{bulk} \times CN_{bulk} + x_{subsurf,step} \times CN_{subsurf,step} + x_{subsurf,ter} \times CN_{subsurf,ter}$$

Here CN_{av} is the average coordination number (Pt-Co or Pt-Pt); CN_{bulk}, $CN_{subsurf,step}$, and $CN_{subsurf,ter}$ are coordination numbers in the bulk and the subsurface layer under a step site and under a terrace, respectively; and x is the corresponding fraction of atoms of a given type (Co or Pt). We compute CN_{bulk} as

$$CN_{bulk,i} = 12 \times y_i$$

Here 12 is a total coordination number in the bulk; y_i is the bulk fraction of a metal i (Pt or Co), as found from the overall nanoparticle composition, minus the number of surface Co atoms (see below). In the subsurface layer under a terrace, metal atoms are in contact with the core Pt-Co alloy (total coordination number 9 for an ideal $Co_3O_2/Pt(111)$ structure) and the Co_3O_2 surface oxide layer on top. Accordingly, the CNs are calculated as

$$CN_{subsurf,Pt-Pt,ter} = 9 \times y_{Pt};$$

$$CN_{subsurf,Pt-Co,ter} = 9 \times y_{Co} + \frac{1}{4} \times 3 + \frac{3}{4} \times 2$$

The factors 1/4 and 3/4 reflect the fact that among every 4 atoms in a subsurface layer of a (4x4) supercell, one is bound to 3 Co atoms and three to 2 Co atoms of a surface oxide. The sublayer CNs under step sites are calculated assuming a Pt(211) geometry, as

$$CN_{subsurf,Pt-Pt,step} = 7 \times y_{Pt};$$

$$CN_{subsurf,Pt-Co,step} = 7 \times y_{Co} + 5$$

Here 7 and 5 are the numbers of non-surface and surface neighbors, respectively.

We estimate the fraction of Pt and Co atoms in each layer by approximating the nanoparticle as a sphere. The total number of atoms is calculated by dividing the particle volume by the volume of a primitive unit cell (dimensions using the XRD-based lattice constant). For a Pt_3Co_2 NC with a 3.7 nm diameter, the number of atoms equals 1827. The number of surface atoms is computed by dividing the particle surface area by a per-atom area in a Pt(111) (4x4) supercell with dimensions corresponding to the Pt_3Co_2 lattice constant. Accordingly, we find the 3.7 nm-particle dispersion to be 36%, close to values obtained with a different method[2]. The number of atoms in the subsurface layer was calculated in a similar fashion using a nanoparticle radius of the actual radius minus the distance between subsurface and surface layers (2.041 Å, as in the $Co_3O_2/Pt(111)$ slab). To obtain the total number of surface Co atoms, we scale the number of 70% of surface sites by a factor of 12/16 to reflect the fact that every 12 Co atoms in a Co_3O_2 honeycomb geometry occupy area equivalent to 16 surface Co (or Pt) atoms in a close-packed configuration. We assume the number of sublayer atoms under step sites to be equal to the number of step sites.

Results of model-based calculations are given in Tables S6 and S7.

Section S3. Relative kinetic stability estimation of Co_3O_2 monolayer at 250 °C, 1 atm H_2 vs. 160 °C, 33 atm H_2

We calculate the vacancy formation rate as

$$r = k_{O+H \rightarrow OH} \theta_{2H}$$

Here $k_{O+H\rightarrow OH}$ is the rate constant for the OH formation reaction; θ_{2H} is the surface coverage of dissociated H_2 molecules. The coverage is found assuming equilibrium between the chemical potentials of an adsorbed state, gaseous H_2 and vacant surface sites (μ_{2H}, $\mu_{H_2,gas}$, and μ_*, respectively):

$$\mu_{2H} = \mu_{H_2,gas} + \mu_*$$

The chemical potentials are expressed in terms of surface coverages and H_2 pressure:

$$\mu_{2H}^0 + RT \ln \theta_{2H} = \mu_{H_2,gas}^0 + RT \ln \frac{P_{H_2,bar}}{1\ bar} + \mu_*^0 + RT \ln \theta_*$$

Here a naught in a superscript denotes quantities at a given temperature (160 or 250 °C) and 1 bar H_2 pressure. The coverage of 2H species is calculated in terms of Gibbs free energy of adsorption $\Delta G_{H_2,ads}$, assuming $\theta_* = 1$, as

$$\theta_{2H} = exp\left(-\frac{\Delta G_{H_2,ads}}{RT}\right) \times \frac{P_{H_2,bar}}{1\ bar}$$

The reaction rate constant is calculated according to the transition state theory:

$$k_{O+H\rightarrow OH} = \frac{k_B T}{h} exp\left(-\frac{\Delta G_{O+H\rightarrow OH}^{\neq}}{RT}\right)$$

Zero point energies and temperature corrections were accounted for in Gibbs free energy calculations by assuming that all surface species only possess vibrational degrees of freedom.

Following homolytic splitting of the H_2 molecule, one H atom transfers to a neighboring O atom to form OH (1.3 eV barrier). A second H atom attacks OH and produces water (1.2 eV barrier), which subsequently desorbs. The transition state of hydroxyl formation, O+H→OH, is the least stable (Figure S8), suggesting OH formation to be the rate-limiting step of a vacancy formation. We find its rate at 160 °C and 33 bar H_2 to be equal to $5.26\cdot10^{-3}$ s^{-1} (Table S8), assuming the catalyst is in equilibrium with the H_2 gas. Under *in situ* XAS conditions (250 °C and 1 bar H_2), the corresponding vacancy formation rate is greater by a factor of two ($1.15\cdot10^{-2}$ s^{-1}). Once formed, the vacancy is easily reoxidized by BHMF-to-HMMF reactions (Table S5, reactions 11-12) with a rate of $4\cdot10^{10}$ s^{-1} (0.2 eV C-O scission barrier). This analysis provides a rationalization as to why the Co_3O_2 surface oxide is stable in a reducing reaction environment.

Section S4. HMF conversion pathways on Pt(111)

Figure S9 shows the reaction network on Pt(111). HMF is hydrogenated to BHMF, which then undergoes dehydroxylation and hydrogenation to DMF and side reactions leading to DMTHF and 2-hexanol (HMF ring hydrogenation is unimportant based on experimental data). The reaction network consists of 31 elementary reactions, including C-H and O-H formation at side groups, C-H formation at the furan ring, C-OH scission, and ring opening via C-O scission. We use first principles-based screening methods to fast-estimate the thermochemistry and reaction barriers[1]. Reactions with highest barriers are subsequently refined using DFT. Results are generally consistent with general knowledge that Pt is a great hydrogenation catalyst of aliphatic hydrocarbons and carbonyl containing compounds (aldehydes and ketones). Dehydroxylation is slow with the barrier of 1.4 eV. The preferred ring-opening path entails the C-O scission followed by hydrogenation of the α-C rather than ring activation followed by ring opening. Ring opening has a moderate barrier of 1 eV. The associated ring closing barrier is only 0.3 eV, suggesting that ring opening is reversible. Subsequent hydrogenations possess a maximum barrier of 1.2 eV, slightly higher than that of ring opening. The preferred sequence for

DMF ring hydrogenation is α_1-C, β_1-C, β_2-C, and α_2-C, regardless of the metal surface, but other sequences are also energetically competitive. The initial hydrogenation barrier is 1.0 eV. Subsequent hydrogenations have barriers of 0.6, 1.0, and 1.0 eV.

References
1.   (a) Vorotnikov, V.; Vlachos, D. G. *J. Phys. Chem. C* **2015,** *119*, 10417-10426;
         (b) Wang, S.; Vorotnikov, V.; Sutton, J. E.; Vlachos, D. G. *ACS Catal.* **2014,** *4*, 604-612.
2.   Pérez, O.-L.; Romeu, D.; Yacamán, M. J. *J. Catal.* **1983,** *79*, 240-241.